Published online 4 January 2021

Nucleic Acids Research, 2021, Vol. 49, No. 3 ***1235–1246***
doi: 10.1093/nar/gkaa1254

Small molecules inhibitors of the heterogeneous ribonuclear protein A18 (hnRNP A18): a regulator of protein translation and an immune checkpoint

Eduardo Solano-Gonzalez[1], Katherine M. Coburn[2], Wenbo Yu[3,6], Gerald M. Wilson[2], Elmar Nurmemmedov[4], Santosh Kesari[4], Elizabeth T. Chang[5], Alexander D. MacKerell, Jr[3,6], David J. Weber[2,5,6] and France Carrier[1,5,*]

[1]University of Maryland, Baltimore, School of Medicine, Department of Radiation Oncology, 655 West Baltimore, Street, Baltimore, MD 21201, USA, [2]University of Maryland, Baltimore, School of Medicine, Department of Biochemistry and Molecular Biology, 108 N. Greene Street, Baltimore, MD 21201, USA, [3]Computer-Aided Drug Design Center, Department of Pharmaceutical Sciences, School of Pharmacy, University of Maryland, Baltimore, 20 Penn Street, Baltimore MD 21201, USA, [4]John Wayne Cancer Institute, 2200 Santa Monica Blvd, Santa Monica, CA 90404, USA, [5]University of Maryland Marlene and Stewart Greenebaum Comprehensive Cancer Center, Baltimore, MD 21201, USA and [6]Center for Biomolecular Therapeutics (CBT), University of Maryland School of Medicine, Baltimore, MD 21201, USA

Received May 01, 2020; Revised December 14, 2020; Editorial Decision December 15, 2020; Accepted December 16, 2020

ABSTRACT

We have identified chemical probes that simultaneously inhibit cancer cell progression and an immune checkpoint. Using the computational Site Identification by Ligand Competitive Saturation (SILCS) technology, structural biology and cell-based assays, we identify small molecules that directly and selectively bind to the RNA Recognition Motif (RRM) of hnRNP A18, a regulator of protein translation in cancer cells. hnRNP A18 recognizes a specific RNA signature motif in the 3′UTR of transcripts associated with cancer cell progression (Trx, VEGF, RPA) and, as shown here, a tumor immune checkpoint (CTLA-4). Post-transcriptional regulation of immune checkpoints is a potential therapeutic strategy that remains to be exploited. The probes target hnRNP A18 RRM *in vitro* and in cells as evaluated by cellular target engagement. As single agents, the probes specifically disrupt hnRNP A18–RNA interactions, downregulate Trx and CTLA-4 protein levels and inhibit proliferation of several cancer cell lines without affecting the viability of normal epithelial cells. These first-in-class chemical probes will greatly facilitate the elucidation of the underexplored biological function of RNA Binding Proteins (RBPs) in cancer cells, including their effects on proliferation and immune checkpoint activation.

INTRODUCTION

A growing number of human diseases, including tumorigenesis, are associated with protein translation deregulation (1). Cancer cells depend on an accelerated rate of protein translation to supply essential nutriments required to sustain constant demands by actively proliferating cells. Strategies to deprive cancer cells of these nutriments are therefore attractive approaches to limit cancer proliferation. In fact, anticancer therapies targeting the protein translation regulator mammalian Target Of Rapamycin (mTOR) highlight the importance of targeting protein translation to limit cancer progression. Inhibitors of the mTOR pathway have shown clear benefit in some cancers such as mantle cell lymphomas, Renal Cell Carcinoma and Tuberous Sclerosis Complex-related tumors, but in most other cancers these inhibitors have rather limited efficacy as single agents (2). Current approaches thus aim at combining chemotherapy with humanized immune checkpoint antibodies, but these approaches also combine the chemotherapy toxicity to immune-related adverse events (IRAE) induced by antibodies. New drugs that could simultaneously target cancer progression and tumor immune response are therefore needed to minimize toxicity to normal cells.

To address this need, we aimed at targeting hnRNP A18, a RNA-Binding Protein (RBP) recently described as a new regulator of protein translation in cancer cells (3). Immunohistochemical studies have shown that RBPs are abnormally expressed in several cancers relative to adjacent normal tissues, and their expression correlates with patient prognosis (4). Accordingly, our data indicate that hnRNP

*To whom correspondence should be addressed. Tel: +1 410 706 5105; Fax: +1 410 706 3260; Email: fcarrier@som.umaryland.edu

A18 is upregulated in most cancer tissues as compared to normal tissues and its down regulation significantly reduces tumor growth in mouse xenograft models (5). hnRNP A18 was originally cloned by hybridization subtraction based on rapid induction in UV radiated CHO cells (6). The human hnRNP A18 was subsequently cloned and characterized (7). The protein was also identified in mice following exposure to mild cold shock and is also known as CIRP for Cold Inducible RNA Binding Protein (8). Under normal physiological conditions, hnRNP A18 is predominantly a nuclear protein but translocates to the cytosol in response to cellular stress such as UV radiation and hypoxia (9–11). In the cytosol, it recognizes a 51-nucleotide signature motif in the 3′UTR of targeted transcripts important for cancer progression. In addition to stabilizing these transcripts, hnRNP A18 increases their translation by interacting with the eukaryotic Initiation Factor 4G (eIF4G), a member of the general translational machinery, to initiate translation at the 5′ UTR (3). hnRNP A18 thus represents a potential therapeutic target for the treatment of cancer.

MATERIALS AND METHODS

Computer-aided drug design

Site Identification by Ligand Competitive Saturation (SILCS)-based techniques (12,13–16) were used for mapping the functional group requirements of hnRNP A18 as required to create a pharmacophore for virtual screening. SILCS has advantages such as including protein flexibility and protein and ligand desolvation effects as compared with traditional CADD methods. The crystal structure of the hnRNP A18 RRM domain (PDB ID: 5TBX) (17) was used to initialize the SILCS simulation. The Reduce software (18) was used to choose optimal Asn, Gln and His side-chain ring orientations and determine the optimal protonation states of His residues. The protein was immersed in a box of water containing eight organic solutes at ∼0.25 M each. These include benzene, propane, methanol, formamide, imidazole, acetaldehyde, methylammonium and acetate. The size of the simulation box was chosen to have the protein extrema separated from the edge by 8 Å on all sides. Ten such protein–aqueous solution–solute systems were generated with each system differing in the initial positions and orientations of the solutes and water to maximize conformational sampling of the aqueous solution and the protein. The SILCS simulations were performed using the MolCal program (SilcsBio LLC) and the GROMACS (19) simulation program with the CHARMM36 force field (20,21), CHARMM general force field (CGenFF) (22,23) and CHARMM TIP3P water model (24) to describe the protein, organic solutes and water, respectively. 3D functional group probability distributions of selected atoms from the organic solutes were extracted from the simulations to construct the FragMaps. The voxel occupancies of the eleven atom types were merged according to their chemical interaction types to create the following FragMap types: (i) generic nonpolar, APOLAR (benzene and propane carbons); (ii) generic neutral donor, HBDON (methanol oxygen, formamide and imidazole amide nitrogen atoms); (iii) generic neutral acceptor, HBACC (methanol, formamide, acetaldehyde oxygens and imidazole neutral nitrogen); (iv) positive donor, MAMN (methylammonium nitrogen); (v) negative acceptor, ACEO (acetate oxygens); (vi) aromatic, BENC (benzene carbons); (vii) aliphatic, PRPC (propane carbons); (viii) MEOO (methanol oxygen); (ix) FORN (formamide nitrogen); (x) FORO (formamide oxygen); (xi) AALO (acetaldehyde oxygen); (xii) IMIN (imidazole neutral acceptor nitrogen) and (xiii) IMIH (imidazole neutral donor protonated nitrogen). These FragMaps types are included by default as previously described (14,15). The voxel occupancies in the FragMaps were normalized and Boltzmann transformed to yield grid free energies (GFE). An exclusion map representing the fragment/water forbidden region from the SILCS simulations was generated to serve as an alternative to describe the protein surface versus the traditional representations of the protein surface. The exclusion map considers protein flexibility in combination with regions that water and the organic solutes can access, thereby describing potential regions to which a ligand may occupy that are under the solvent accessible surface on the target protein that are inaccessible based on the crystal structure alone. To search for potential hnRNP A18 small molecule inhibitors targeting the RNA binding pocket, the SILCS-Pharm protocol (16) was used to develop pharmacophore models for virtual screening. In addition, the SILCS exclusion map was also used in the model to represent the forbidden region that ligands cannot occupy. Pharmacophore based virtual screening was performed using Pharmer (25) against the University of Maryland CADD Center in silico database that contains 721 368 compounds (1 695 786 molecules considering different protonation states and tautomers) from the vendor Chembridge and 56 237 compounds (126 575 molecules) from the vendor Maybridge. The 154 compounds for experimental assays were selected based on the root-mean-square difference of the ligand pharmacophore points with the SILCS-Pharm features, chemical diversity based on BIT-MACCS chemical fingerprint cluster using MOE (Chemical Computing Group), predicted bioavailability considerations and commercial availability. A similarity screen target the query compound Chembridge 7858888 was performed against the full UMB CADD Center 5.04 million compound database using BIT-MACCS chemical fingerprints with the program MOE. The similarity cut-off value was set at 80% and 264 compounds were identified based on those criteria.

PAMPA. The Parallel Artificial Membrane Permeability Assay (PAMPA) was performed by Pion (Billerica, MA) on 81 compounds selected out of the 264 compounds showing at least 80% similarity to Chembridge 7858888, log P <5.0 as calculated using the Molecular Operating Environment program (Chemical Computing Group), and four-dimensional bioavailability (4DBA) closer to 0 (>–4.9) (26). The compounds were dissolved at 10 mM in dimethyl sulfoxide (DMSO, spectrophotometric grade) and filtered (0.2 μm pore size, hydrophylic PVDF). The assays were carried in PAMPA STIRWELL™ plates (lot A0440) and measured at pH 5.0 and 6.8 at room temperature for ∼4 h on a PAMPA Evolution™ instrument. After permeation, a UV spectrum was scanned from 245 to 498 nm to determine the relative concentration in both the donor (GIT-0 lipid (PN 110669, lot# 520552) and acceptor sink buffer (PN 110139,

lot# 520549). The effective permeability (Pe $\times$ 10^{-6} cm/s) coefficients were then calculated from these results (27).

NMR: ^{15}N-labeled A18 RNA recognition motif purification

^{15}N-labeled and ^{13}C,^{15}N-double labelled hnRNP A18 RNA Recognition Motif (RRM) (residues 1–92 of hnRNP A18 wildtype) was expressed and purified (>99%) with methods similar to those described previously (17). Briefly, the hnRNP A18 RRM construct was cloned into the *Escherichia coli* expression plasmid pHGK-IF (unpublished) in-frame with a 6x-His-tagged protein G, B1 domain (GB1) fusion protein and *Tobacco etch virus* (TEV) protease-cleavage site upstream. The pHGK-A18 RRM construct was transformed into *E. coli* BLD21(DE3) cells and a single colony was grown in 5 l of M9 minimal medium (28) with ^{15}N-labeled (>99%) ammonium chloride as the single nitrogen source at 37°C. Double-labelled ^{13}C–^{15}N-labeled preparations were grown using ^{15}N-labeled ammonium chloride (>99%) and $^{13}C_6$-labeled glucose (>99%) as the only nitrogen and carbon sources, respectively. When the A_{600} reached 0.8, the incubation temperature was reduced to 18°C. His_6GB1-A18 RRM expression was induced by the addition of 1 mM IPTG (isopropyl β-D-1-thiogalactopyranoside) and cells were grown for an additional 16 h at 18°C. Cells were pelleted by centrifugation at 10 000 g for 20 min. The cells were resuspended in a denaturing buffer (20 mM Tris pH 7.4, 500 mM NaCl, 5 mM imidazole, 6 M urea and 0.5 mM AEBSF) and lysed via sonication. The cells were centrifuged for 18 000 g for 45 min to pellet cellular debris and the supernatant was filtered with a 0.45 μm syringe. The filtered supernatant was applied to a 5 ml HisTrap FF column (GE Healthcare, catalog No. 17-52255-01), which was equilibrated with the denaturing buffer. A refolding buffer (20 mM Tris pH 7.4, 500 mM NaCl, 5 mM imidazole) was applied to the column as a linear gradient over 20 column volumes (100 ml). His_6GB1-A18 RRM was eluted from the column through a linear gradient of elution buffer (20 mM Tris pH 7.4, 500 mM NaCl, 500 mM Imidazole) over 10 column volumes (50 ml). The eluted fractions were analysed by SDS-PAGE and fractions with His_6GB1-A18 RRM were combined, dialyzed into the refolding buffer (see above) overnight, and treated with His-tagged TEV protease simultaneously to remove A18 RRM from the His_6GB1 fusion protein. The sample was applied to a HisTrap HP column (GE Healthcare, catalogue no. 17-5247-01) in refolding buffer and the flow through contained purified hnRNP A18 RRM. The protein was dialyzed into ultrapure water, concentrated using Amicon Ultra centrifugal filter units with a 3 kDa molecular weight cut off, and quantified by the Bio-Rad Protein Assay (Bio-Rad Inc., Hercules, CA). The hnRNP A18 RRM was stored at a concentration of ~0.33 mM in ultrapure water at −80°C until use.

NMR spectroscopy

The hnRNP A18 RRM samples used for compound screening via high field NMR spectroscopy contained 0.1–0.2 mM ^{15}N-labeled hnRNP A18 RRM, ultrapure water, 10% D_2O, 5% d_6-DMSO and up to 5 mM of each of the forty compounds tested, as based on their solubility. All the 2D ^{15}N-edited HSQC data were collected at 25°C with a Bruker Avance 800 US2 NMR spectrometer (800.27 MHz, ^{1}H) equipped with pulsed-field gradients, four frequency channels, an automatic sample changer, and a TXI cryogenic probe. Backbone chemical shift assignments for the RRM domain of hnRNP A18 were obtained using standard heteronuclear multidimensional NMR experiments for double labelled ^{13}C–^{15}N-labeled hnRNP A18 RRM and deposited in the Biological Magnetic Resonance Database (BRMB; access number 28117). Backbone resonance assignments in the presence of compounds were achieved via compound titrations and monitoring chemical shift changes until solubility limits were reached (<5 mM compound). Data were processed with NMRPipe (29), and proton chemical shifts and their perturbations upon binding the various compounds were reported with respect to the H_2O or HDO signal taken as 4.698 ppm relative to external TSP (0.0 ppm).

Compounds titrations: Chembridge 7858888, Chembridge 7646184, Chembridge 6823240 and VITAS STK508411 were titrated into 0.15 mM A18 RRM at concentrations of 0, 0.075, 0.15 and 0.30 mM. Chemical shift perturbations were observed via ^{1}H,^{15}N-edited HSQC. All titrations were performed in 20 mM Tris pH 9.0, 10% D_2O and 5% D_6MSO at 37°C, and collected with a Bruker Avance 800 US2 (800.27 MHz NMR spectrometer equipped with pulsed-field gradients, four frequency channels, and a TXI cryogenic probe).

Measurement of RNA binding activity *in vitro*

RNA substrates. RNA oligonucleotides were synthesized and purified by Integrated DNA Technologies, Dharmacon (Skokie, IL). Lyophilized pellets were resuspended in 10 mM Tris (pH 8.0). RNA concentrations and fluorophore labelling efficiencies were quantified by absorbance, incorporating fractional contributions from fluorescein (Fl) labels to A_{260} as described (30). RNA probe sequences are listed in Table 1.

RNA band shift (EMSA)

Recombinant human His-hnRNP A18 was purified as described before (9) except that bacteria were grown at 30°C, recombinant human His-hnRNP A1 was obtained by subcloning the human open reading frame (NM_002136) from hnRNPA1 Myc-DDK-tagged plasmid (RC203314, OriGene Technologies Inc, Rockville, MD) into pEX-C-His vector (OriGene Technologies) in the BseR 1/Mlu1 restriction sites by PCR. The recombinant protein was purified from bacteria grown at 30°C with a His-tag purification kit (His-Bind, Millipore Sigma, Burlington, MA) according to the manufacturer's recommendations. Recombinant human His-hnRNP F was purified from bacterial expression of vector pET-15b-hnRNP-F (Addgen, Watertown, MA) and purified as described before (31). RNA band shifts were performed according to the manufacturer recommendations (LightShift Chemiluminescent RNA EMSA kit, Thermo Scientific, Rockford, IL). Briefly recombinant proteins (1

Table 1. RNA probe sequences for Fluorescence Anisotropy and EMSA assays

Name	Sequence (5′→ 3′)
hnRNP A18 motif 1 Fl	GCAGAUCCAGGGUGGGAUUUUCUUGAGGAAGUUACAAAUAAGCUUGUUACA-FluorT
hnRNP A18 motif 1 Biotin	GCAGAUCCAGGGUGGGAUUUUCUUGAGGAAGUUACAAAUAAGCUUGUUACA-Biotin
IRE 51 nt Biotin	UCCUGCUUCAACAGUGCUUGGACGGAACUCCUGCUUCAACAGUGCUUGGAC-Biotin
IRE 28 nt Biotin	UCCUGCUUCAACAGUGCUUGGACGGAAC-Biotin
hnRNP A1 motif Biotin	UAUGAUAGGGACUUAGGGUG-Biotin
hnRNP F motif Biotin	UUAGGGUUAGGGUUAGGGUUAGGGUUAGGGUUAGGGUUAGGGUUAGGG-Biotin

μg) were incubated in the presence or absence of the indicated compound for 10 min followed by 10 min incubation in the presence of their respective biotinylated consensus RNA binding motif (Table 1: (11,32,33)) at room temperature in 20 μl and run on native polyacrylamide gels transfer to nylon probes and hybridize with streptavidin HRP antibody.

RNA-IP

The RNA-IP was performed on PC-3 cell extracts with the Magna RIP RNA-Binding Protein Immunoprecipitation Kit (Millipore Sigma, Burlington, MA) as recommended by the manufacturer.

CTLA-4 primers:
5′>TGACAGCCAGGTGACTGAAG<3′;
5′>GCCTCAGCTCTTGGAAATTG<3′. The size of the amplified product was 493 for CTLA-4.

GAPDH primers:
5′>ACATCAAGAAGGTGGTGAAGCAGG<3′;
5′>CCAGCAAGGATACTGAGAGCAAGAG <3′. The size of the amplified product was 324 for GAPDH.

Fluorescence anisotropy

Quantitative assessments of hnRNP A18-RNA binding equilibria were performed using fluorescence anisotropy essentially as described previously (30). Briefly, binding reactions (100 μl) were assembled as described for RNA band shift (EMSAs) but in absence of glycerol and using fluorescein labelled rather than biotin labelled RNA substrates. Reactions were incubated at 25°C for 30 min; preliminary kinetics runs verified that equilibrium was attained within this period. Subsequently, total reaction anisotropy (At) and fluorescence intensity were measured using a Beacon 2000 Fluorescence Polarization System (Panvera) equipped with a 490-nm excitation filter and a 535-nm emission filter. Drug-dependent changes in A_t were analysed by nonlinear regression using the four-parameter logistic equation (1) and PRISM software (GraphPad).

$$A_t = A_R + \frac{A_{PR} - A_R}{1 + 10^{\log(IC_{50}/[drug])\cdot h}} \quad (1)$$

Here, A_{PR} represents the intrinsic anisotropy of the protein:RNA complex in the absence of tested compounds, A_R is the anisotropy of the RNA ligand in the absence of protein, [drug] is the concentration of each tested compound and *h* is the Hill slope.

CAT ELISA

CAT-ELISA was performed as recommended by the manufacturer (Sigma-Aldrich). Briefly, human melanoma LOX-IM VI cells stably transfected with hnRNP A18-GFP (9) were transiently transfected with a CAT reporter vector harboring TRX 3′UTR (34). Twenty-four hours later, the cells were distributed in six-well plates and treated with increasing amount of the chemical probes. The next day, the cells were washed, and protein extracted. The CAT-ELISA was performed on 25 μg of proteins in triplicate in microplates precoated with a polyclonal antibody for CAT and revealed with anti-CAT-DIG, anti-DIG-POD and the peroxidase substrate ABTS as recommended. Cleavage of the substrate catalysed by the peroxidase enzyme was measured on a plate reader at 405 nm.

Cell viability and tumor growth in vivo. Cells viability was measured on normal human mammary epithelial cells (HMEC: ATCC, Gaithersburg, MD) grown as recommended by the manufacturer and human cancer cells including melanoma LOX-IM-VI, colon cancer RKO, Glioblastoma D54, pancreatic cancer MiaPaca and triple negative breast cancer MDA-MB-231 cells (5). Down regulation of hnRNP A18 was performed as described before (5) in the LOX-IM-VI and MDA-MB-231 cells with the exception that clonal expansion was performed by serial dilution of the transfected cells. Viability was measured with the Apo-Tox-Glo kit (Promega, Madison, WI) as recommended by the manufacturer. The cells were plated (10 000 cells per well) on a 96-well plate and exposed to increasing concentration of chemical probes for 24 h and reacted with the viability reagent as recommended. Fluorescence was measured on a plate reader at 400 nm Ex/505 nm Em.

Tumor growth *in vivo* was performed as described previously (5) with the assistance of the University of Maryland Marlene and Stewart Greenebaum Comprehensive Cancer Center Translational Laboratory Shared Services, reviewed and approved by an Institutional Animal Care and Use Committee (Protocol # 1016012) at the University of Maryland Medical School. Briefly, NRG mice were injected through the tail vein with 1×10^6 human breast cancer MDA-MB-231 cells expressing the firefly luciferase gene and either scrambled shRNA or shRNA hnRNP A18. Following injection, mice were injected intraperitoneally with Luciferin (150 mg/kg, Perkin Elmer) at the indicated time point and imaged with a Xenogen IVIS optical imager 10

min later under anesthesia (2% isoflurane gas). Total photon flux (photons/sec) was calculated using Living Image 3.0 software.

Cellular thermal shift assay (CETSA)

Cellular thermal shift assay (CETSA) was performed with LOX-IM-VI hnRNP A18 cells cultured in RPMI medium supplemented with 10% FBS. For an initial determination of the melting profile of hnRNP A18, cells dispensed into 96-well PCR plate in the above medium (5000 cells/well/50 μl), were subjected to temperature gradient (40–60°C) for 10 min. Cold non-denaturing lysis buffer (PBS supplemented with 0.1% Triton X-100 and 1× protease inhibitors) was added to wells, and the plate was rocked and incubated for 15 min on ice. Subsequently, centrifugation was performed at 14 000 rpm to sediment the unstable protein content. Supernatant was collected, and SDS-PAGE gel was run, and immuno-detection was performed using polyclonal anti-hnRNP A18 antibody (Sigma, CIRP). hnRNP A18 band was quantified on LI-COR C-Digit Blot Scanner, and subsequently $T_{agg}(50)$ and $T_{agg}(75)$ values were calculated for hnRNP A18. In a subsequent run, cells were treated at various doses (80, 40, 20, 10, 5, 2.5 and 1.25 μM) of VITAS STK508411, Chembridge 7646184 and OTAVA 2192853 together with DMSO control, for 3 h. Cells were then subjected to heat shock at $T_{agg}(75)$ for 10 min, and unstable protein was removed by centrifugation step. Following an immuno-blotting step, bands of stable hnRNP A18 protein was quantified, normalized to loading control and plotted using GraphPad Prism software. EC_{50} values of VITAS STK508411, Chembridge 7646184 and OTAVA 2192853 compounds were calculated.

RESULTS

Site Identification by Ligand Competitive Saturation (SILCS) and experimental validation via NMR

hnRNP A18 contains an Arginine Glycine rich (RGG) domain and a single RNA Recognition Motif (RRM) rather than the two canonical RRMs found in most hnRNP proteins (3). While the RGG is disordered, the RRM is structured and a crystallographic structure is available of the apo protein ((17), PDB ID: 5TBX). To identify the regions of the protein interacting with the RNA, the structure of hnRNP A18 RRM was aligned with the crystal structure of a similar hnRNP, hnRNP A1 (PDB ID: 5MPL, (35) in a complex with a short RNA oligonucleotide (ODN) from which a model of the hnRNP A18-ODN complex was obtained (Figure 1A-B). This indicated residues F10, F50, F52 and R48 on hnRNP A18 to be important residues for RNA binding (17) such that inhibitors targeting binding in this region would be expected to block hnRNP A18–RNA interactions (Figure 1C).

We used a state-of-the-art Computer Aided Drug Design (CADD) algorithm, Site Identification by Competitive Ligand Saturation (SILCS, (12)) (Figure 1C–F) for inhibitor identification. Step one of SILCS involves calculation of 3D maps of functional group affinity patterns on the entire protein surface, termed FragMaps, initiated from the 3D crystallographic structure of hnRNP A18 RRM (17). Analysis of the FragMaps in the targeted binding region on the protein surface (Figure 1C) in which the modelled ODN is included show negative FragMaps corresponding to the phosphate groups in the region of R48 with aromatic and aliphatic FragMaps near residues F10, F50 and F52 that are overlapping with the sugars and bases of the ODN (Figure 1C). This pattern of FragMaps corresponds with the types of functional groups present in drug-like molecules and, accordingly, were deemed suitable to guide the identification of potential hnRNP A18–RNA inhibitors.

SILCS database screening was initiated by determining a four-point pharmacophore model based on the FragMaps to be used in virtual screening for small molecules that can potentially bind to hnRNP A18 (Figure 1D, (16)). The 4 points value used in this model is the optimized value as described in (16). The pharmacophore for hnRNP A18 has three aromatic features and one anionic feature. These four pharmacophore features capture the main crystal binding mode of RNA which is predicted to be important for inhibitor binding (Figure 1B). A virtual screen against the UMB CADD Center database of commercially available compounds (∼780 000 molecules) identified 154 molecules with the correct number, types, and spatial relationship of the pharmacophore features. Figure 1E shows the SILCS predicted binding pose of the best hit compound (Chembridge 5224046) to recapitulate the pharmacophore model used for virtual screening. In addition, the binding pose of Chembridge 5224046 mimics the hnRNP A1 RNA binding mode (Figure 1F).

The top 154 compounds were then selected using the Pharmer RMSD score which measures the spatial similarity between the screened molecules and the query pharmacophore model. From these 154 compounds, 40 were selected based on chemical diversity and bioavailability considerations and obtained from commercial sources. The compounds were then screened by NMR and twenty seven of the 40 compounds perturbed chemical backbone shift values for hnRNP A18 RRM, as illustrated for Chembridge compound 7858888 (Figure. 2A, Supplementary Figure S1 and Supplementary Table S1). The majority of the 'hit' compounds affected a similar set of residues with many of the perturbed residues clustered within a similar location on the RRM. While backbone ^{H}N correlations for all the residues important for RNA binding were significantly perturbed (i.e. F9, R47, F49, F51) consistent with the inhibitor binding in this region, correlations for backbone resonances outside the RRM were also perturbed, providing evidence that these molecules induce changes in conformation beyond the RNA binding motif of hnRNP A18 (Figure 2A, E, Supplementary Figure S1). The NMR chemical shift perturbation data for these compounds is consistent with (i) their blocking the RRM domain directly and (ii) changing the overall conformation of hnRNP A18, and it is likely that both attributes are important for their inhibitory properties.

Validation of RNA binding inhibition and specificity

To determine whether Chembridge 7858888 affected hnRNP A18 RNA binding activity we performed fluorescence anisotropy competition binding experiments. As shown in

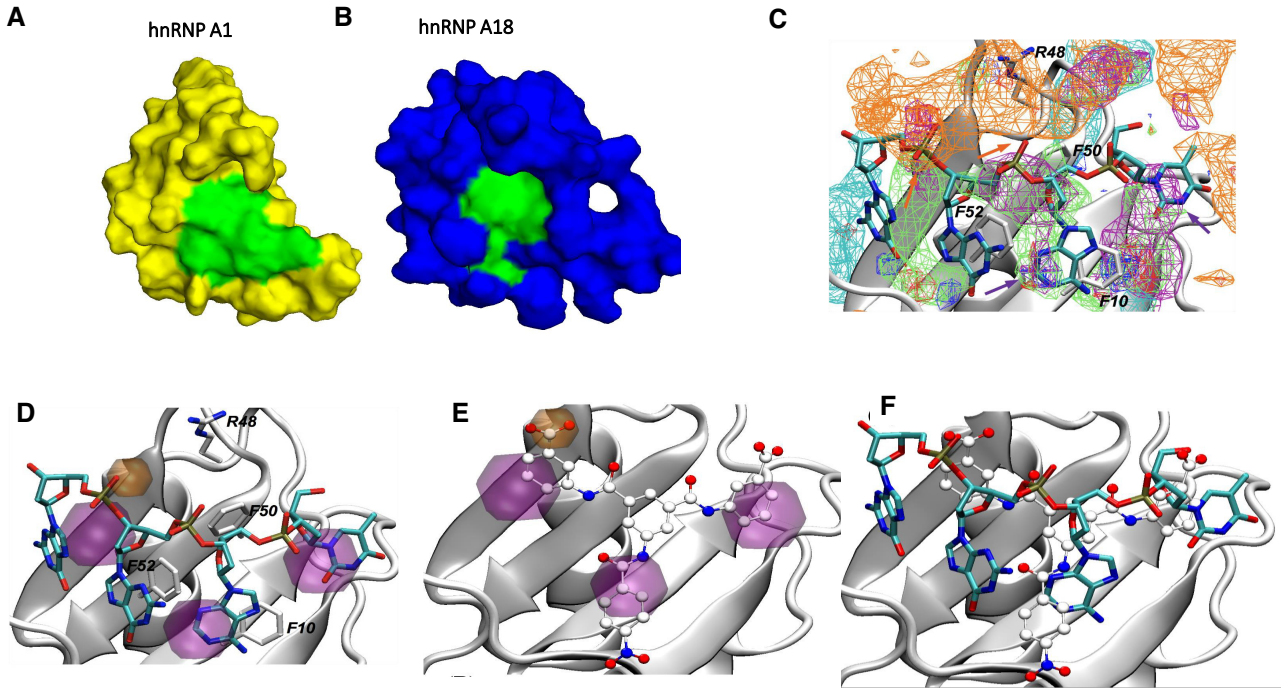

Figure 1. Site-Identification by Ligand Competitive Saturation (SILCS) to identify potential small molecule inhibitors to disrupt hnRNP A18–RNA interactions. (**A**, **B**) Surface representations of the crystal structures of the RRM of hnRNP A1 (A; yellow) bound to RNA (green) and hnRNP A18 (B; blue) with residues predicted to bind RNA (green). (**C**) SILCS FragMaps overlaid on the structure of the hnRNP A18 RRM domain. Aliphatic, aromatic, hydrogen bond donor, acceptor, positively charged and negatively charged FragMaps are contoured at –1.2 kcal/mol GFE values and are colored in green, purple, blue, red, cyan and orange, respectively. Protein residues at the binding region are also shown and labeled. Bound RNA modelled by the alignment of hnRNP A1 with hnRNP A18 is also shown. (**D**) Pharmacophore model derived using SILCS-Pharm based on FragMaps for virtual screening. Aromatic and negatively charged pharmacophore features are colored by purple and orange respectively. (**E**) Predicted inhibitor aligned with the pharmacophore model on the crystal structure of hnRNP A1 alone and (**F**) with the modelled RNA structure.

Figure 2I, the compound prevented hnRNP A18 from binding to its targeted RNA in a dose-dependent manner with an IC_{50} of 6.4 μM. Subsequent RNA band shift indicated Chembridge 7858888 outcompeted hnRNP A18 RNA consensus motif but its specificity decreased at higher concentration (data not shown). To bolster specificity, affinity and potential bioavailability, we performed a chemical fingerprint similarity search based on Chembridge 7858888 against the UMB CADD Center *in silico* 5.04 million compound database from which 264 compounds were selected. Of those, 81 compounds were selected based on log *P* and 4DBA (bioavailability) (26) and tested for cell permeability (Parallel artificial membrane permeability assay; PAMPA) (data not shown). Twenty compounds showing higher effective permeability values (Pe > 20) were subsequently tested for hnRNP A18 specificity by RNA band shifts. Four compounds (Patent pending), Chembridge 6823240, Chembridge 7646184, VITAS STK508411 and OTAVA 2192853 (Supplementary Figure S2), met our cell permeability requirements (Pe > 20) and specifically bound hnRNP A18. Chemical shift perturbations were observed for hnRNP A18 RRM in the presence of Chembridge 6823240, Chembridge 7646184 and VITAS STK508411 (Figure 2B–D and Supplementary Figure S3). Chemical shifts in the presence of OTAVA 2192853 could not be determined due to insolubility at higher concentration. Addition of Chembridge 7646184 and VITAS STK508411 produced similar chemical shift perturbations in amino acid residues Q81, M65, S85, S86, S48 and S16. Chembridge 6823240 induced chemical shift perturbations in Q81, but also I13 and S14. However, further investigation is required to determine the exact mode of interaction between these compounds and hnRNP A18 RRM. Chemical shift perturbations mapped onto the hnRNP A18 RRM X-ray crystal structure indicate that Chembridge 7858888 induced much stronger (Figure 2A, E) and non-specific perturbations as compared to chemical shifts induced by Chembridge 7646184, Chembridge 6823240 and VITAS STK508411 (Figure 2E–H).

The compounds capacity to disrupt hnRNP A18 RNA binding activity was confirmed by fluorescence anisotropy (Figure 2I–L) where IC_{50s} between 2.9 and 15 μM were determined. RNA binding specificity was then evaluated on hnRNP A18 and a related hnRNP, hnRNP A1 as well as on a quasi-RRM (qRRM) binding protein hnRNP F. Our data indicate that the chemical probes disrupt hnRNP A18 RNA binding activity (Figure 3A–D) but not the RNA binding activity of hnRNP A1 and hnRNP F, at a concentration five times higher than the VITAS STK508411 IC_{50} (Figure 3F–G, 2L). To further validate the specificity of the chemical probes we evaluated their toxicity on cancer cells depleted of hnRNP A18 (Figure 4A, F). Data shown in Figure 4 indicate that all compounds significantly reduce cells viability more efficiently in human melanoma LOX-IM-VI (Figure 4B–E) and breast cancer MDA-MB-231 (Figure 4G–J) cells expressing hnRNP A18 than in cells depleted of hnRNP A18.

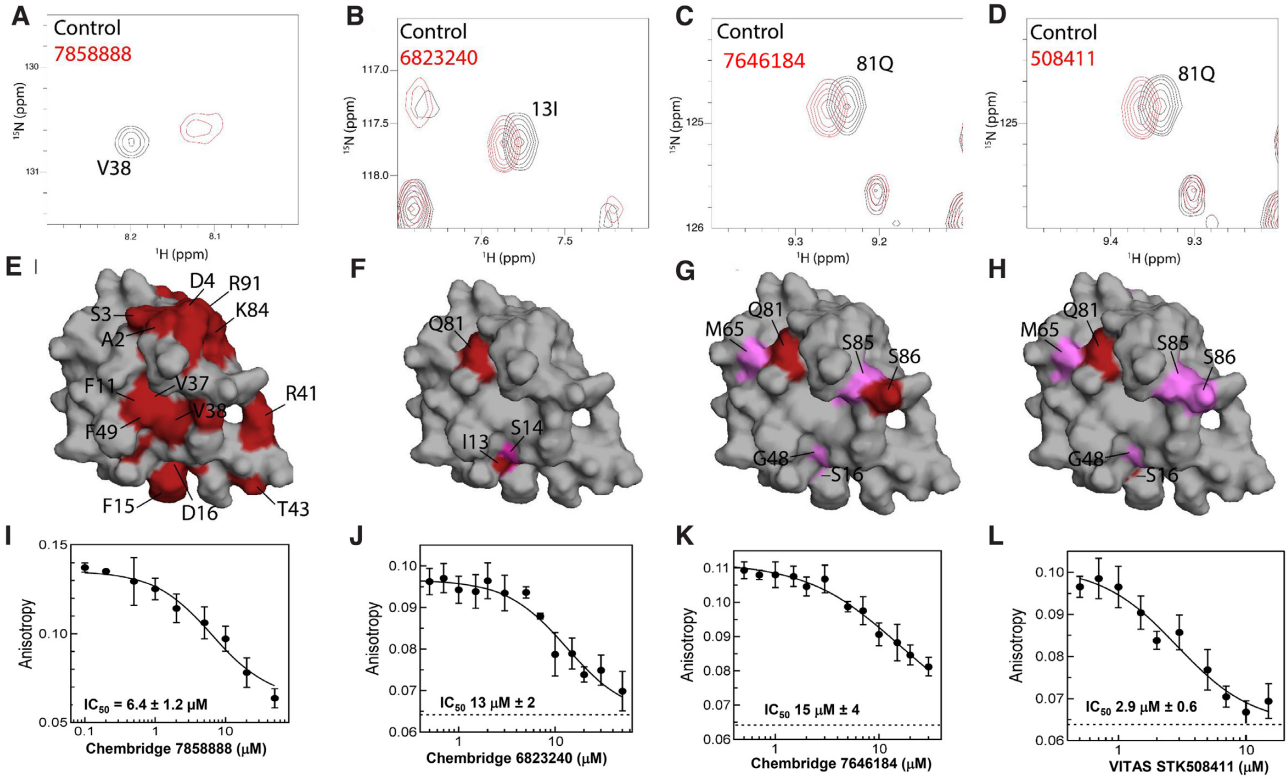

Figure 2. Compounds directly bind to hnRNP A18. Chemical shift perturbations for (**A**) V38 of hnRNP A18 RRM in the presence of Chembridge 7858888, (**B**) for I13 in the presence of Chembridge 6823240, (**C**) for Q81 in the presence of Chembridge 7646184, (**D**) for Q81 in the presence of VITAS STK508411. (E–H) Chemical shift perturbations mapped onto hnRNP A18 RRM X-ray crystal structure for (**E**) Chembridge 7858888, (**F**) Chembridge 6823240, (**G**) Chembridge 7646184, (**H**) VITAS STK508411. Strong chemical shifts are noted in red, while more moderate chemical shifts are demonstrated in pink. (I–L) Fluorescence anisotropy measured for reactions containing recombinant GST-full length hnRNP A18 and Fluorescein tag hnRNP A18 RNA motif 1 in presence of increasing concentrations of (**I**) Chembridge 7858888 (IC_{50} 6.4 μM), (**J**) Chembridge 6823240 (IC_{50} 13 μM), (**K**) Chembridge 7646184 (IC_{50} 15 μM), (**L**) VISTAS STK508411 (IC_{50} 2.9 μM). Error bars indicate standard deviations, $n = 3$.

To verify that these compounds can reach their target (hnRNP A18) in cells, we performed a Cellular Engagement Thermal Shift Assay (CETSA) on three of these compounds in human melanoma cells. The data shown in Figure 5A indicate that VITAS STK508411, Chembridge 7646184 and OTAVA 2192853 can bind to and stabilize hnRNP A18 in human cells with EC_{50} values of 23.8, 4.7 and 2.7 μM, respectively, at 57°C, a temperature that melts hnRNP A18 in absence of compound (Supplementary Figure S4). To determine whether hnRNP A18 binding to these compounds disrupted its cellular functions, we developed a cell-based assay as a read out for hnRNP A18 RNA binding activity. We engineered a reporter vector harboring a hnRNP A18 targeted 3′UTR (TRX; (34)) downstream of a CAT gene. Binding of hnRNP A18 to the targeted 3′UTR is expected to stabilize the CAT transcript and increase CAT protein production, which is then measured by ELISA. Our data (Figure 5B) indicate that the four compounds that competed hnRNP A18 RNA binding activity *in vitro* (Figure 3) also reduced the production of the CAT protein, suggesting that indeed the compounds disrupted hnRNP A18 binding to its targeted transcripts in cells. On the other hand, a different OTAVA compound, 2192700, which has poor aqueous solubility as determined by PAMPA (data not shown), could only reduce CAT protein levels at the highest concentration.

To verify that the four active compounds affected the production of the targeted transcripts in cells, we performed western blot analysis following exposure of melanoma LOX IM VI cells to these compounds. Figure 5C–F indicates that indeed all four compounds disrupted Thioredoxin protein level in a dose dependent manner to levels similar to what was achieved when hnRNPA18 is down regulated with shRNA (Figure 5G, (5)).

Our data indicate that the hnRNP A18 RNA recognition motif is also located in the 3′UTR of the immune checkpoint transcript CTLA-4 (Figure 6A). The hnRNP A18 RNA recognition motif has been described before (11) and sequence alignment of six possible version of the motif are shown (Figure 6A). The motif found in CTLA-4 3′UTR is located between nucleotide 1319 and 1370 relative to the 3′-UTR start site (Figure 6A) and has ∼80% (41/51 nucleotides) similarity to the consensus recognition motifs (Figure 6A). In addition, five of the six invariant nucleotides are conserved (red boxes, Figure 6A). To validate the hnRNP A18 recognition motif in CTLA-4 transcript we performed RNA-IP in human prostate cancer PC-3 cells. The RNA IP was performed as described previously (34,11) under conditions that preserve RNA–protein interaction on polysomes. Data shown in Figure 6B indicate that indeed hnRNP A18 can bind to CTLA-4 transcript on polysomes.

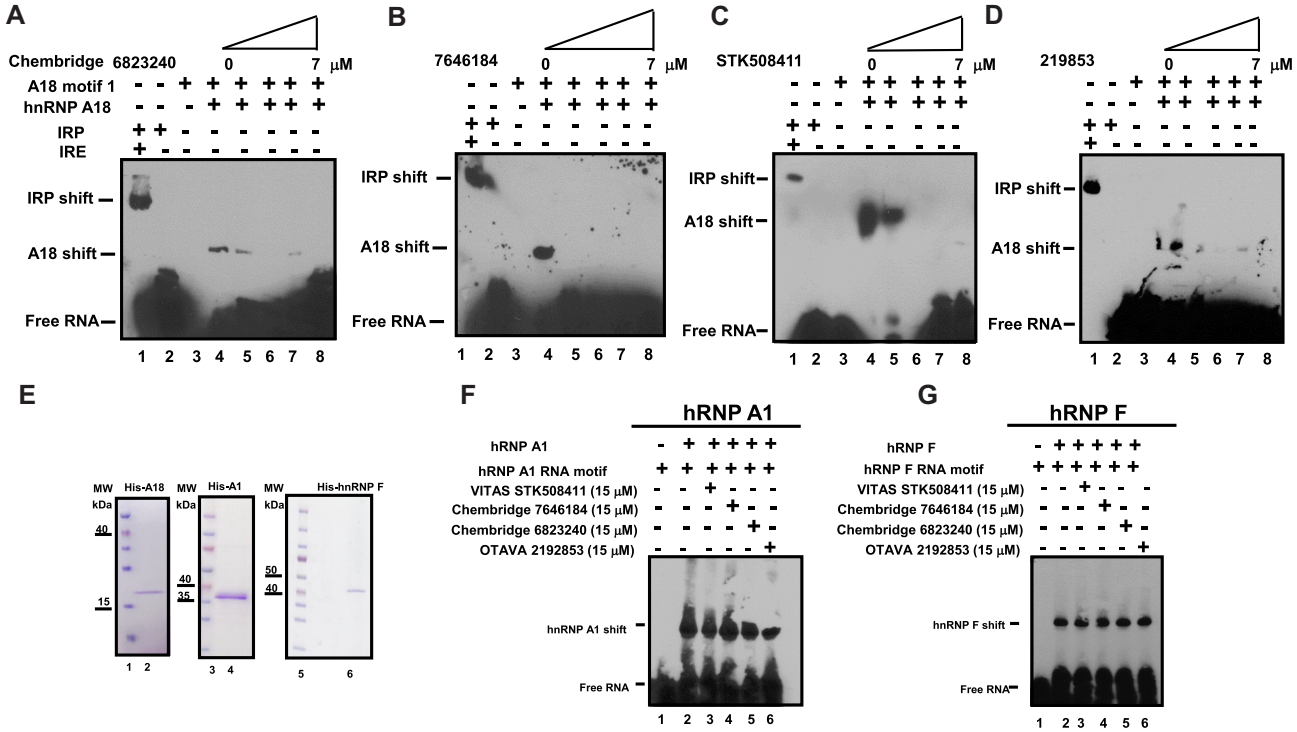

Figure 3. Compounds specificity *in vitro*. (A–D) RNA band shift performed with recombinant full length His-hnRNP A18 incubated with increasing concentration of (**A**) Chembridge 6823240, (**B**) Chembridge 7646184, (**C**) VITAS STK508411, (**D**) OTAVA 219853 and the biotinylated hnRNP A18 RNA consensus motif 1 (Table 1). The Iron Responsive Protein (IRP) in the presence of biotinylated Iron Responsive Element (IRE) is used as a positive control. (**E**) Coomassie blue staining of recombinant His-hnRNP A18 (His-A18, lane 2), His-hnRNP A1 (His-A1, lane 4) and His-hnRNP F (lane 6). Molecular weight (MW) markers are indicated (lanes 1, 3, 5). (**F–G**) RNA band shift performed with either recombinant full length His-hnRNP A1 or His-hnRNP F incubated with their respective biotinylated RNA consensus motif (Table 1) and the indicated compounds (15 μM).

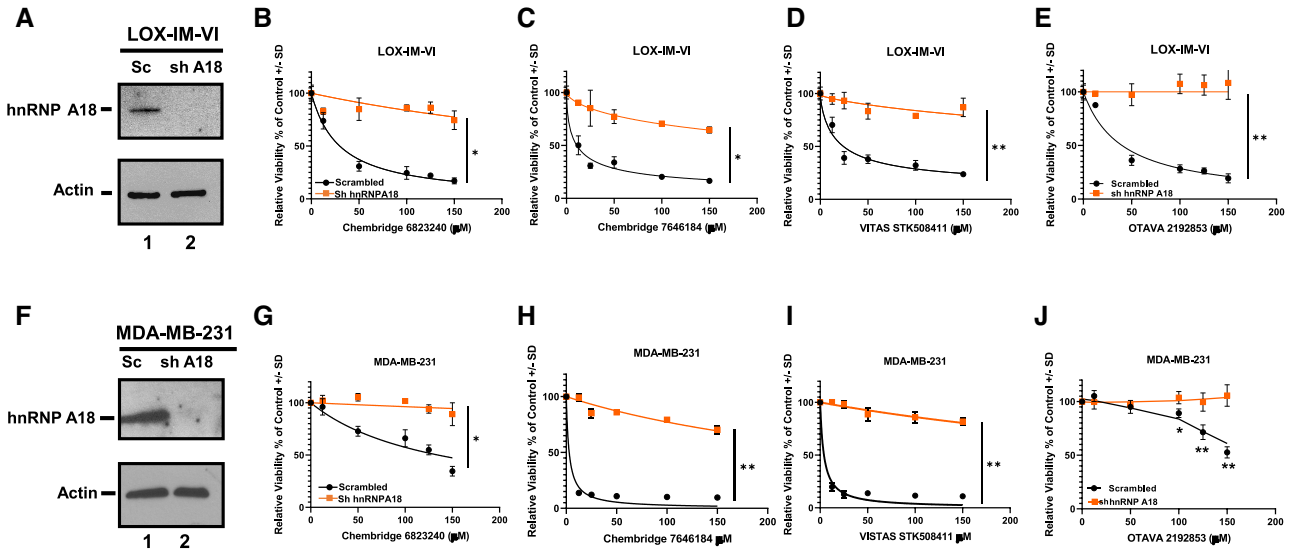

Figure 4. Compounds specificity in cells. (**A**) Western blot analysis performed on LOX-IM-VI cells transfected with either scrambled shRNA or shRNA hnRNP A18 (sh A18). Actin is used as a loading control. (**B–E**) Viability assays performed on LOX-IM-VI transfected with either scrambled shRNA (black lines) or shRNA hnRNP A18 (orange lines) and exposed to increasing concentration of the indicated compound. (**F**) Western blot analysis performed on MDA-MB-231 cells transfected with either scrambled shRNA or shRNA hnRNP A18 (sh A18). Actin is used as a loading control. (**G–J**) Viability assays performed on MDA-MB-231 transfected with either scrambled shRNA (black lines) or shRNA hnRNP A18 (orange lines) and exposed to increasing concentration of the indicated compound. $*P < 0.05$, $**P < 0.005$ performed with GraphPad Prism, *t*-test of the means.

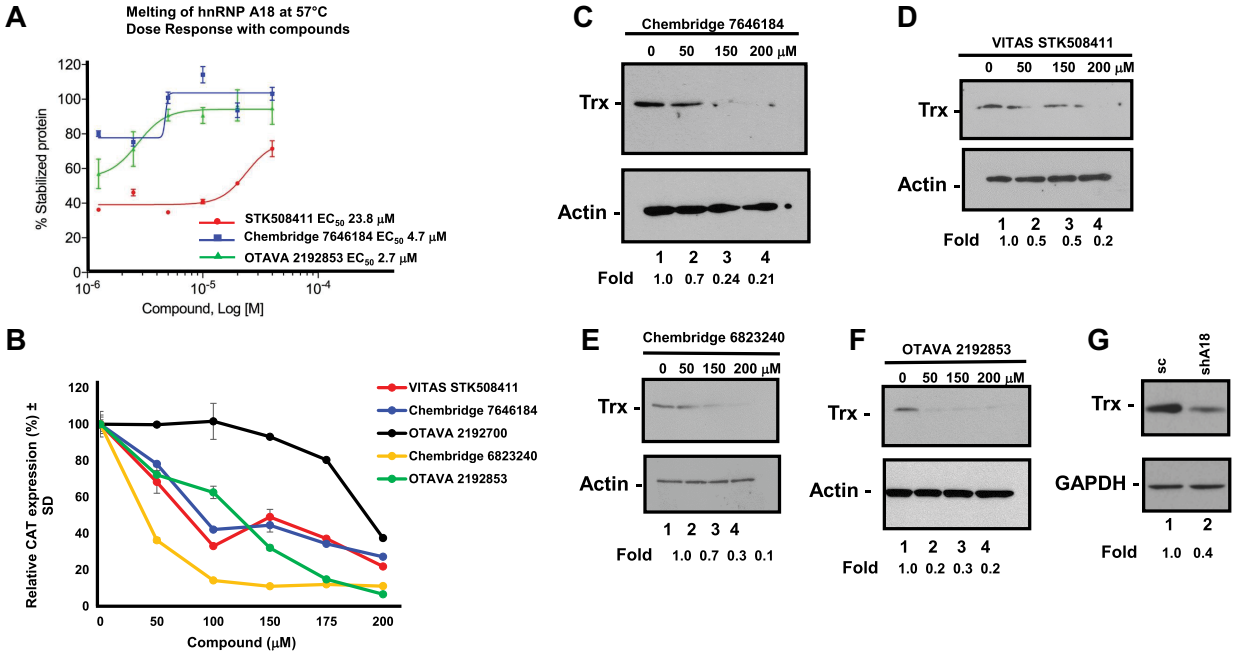

Figure 5. Compounds reach their target, hnRNP A18, in cells and disrupt its RNA binding activity. (**A**) Cellular Engagement Thermal Shift Assay (CETSA). Dose response of hnRNP A18 protection from melting at 57°C in the presence of increasing concentrations of the indicated compounds. CETSA was performed in LOX-IM-VI cells over expressing GFP-hnRNP A18 in presence of VITAS STK508411 (red line), Chembridge 7646184 (blue line) or OTAVA 2192853 (green line). EC_{50} of each compound is indicated. (**B**) CAT-Trx 3′UTR reporter assay. Relative expression of CAT protein detected by ELISA in the presence of increasing concentrations of VITAS STK508411 (red line), Chembridge 7646184 (blue line), Chembridge 6823240 (yellow line), OTAVA 2192700 (black line) or OTAVA 2192853 (green line). Error bars indicate standard deviation, $n = 3$. (**C–F**) Western blot analysis of LOX-IM-VI cells treated with increasing concentrations of the indicated compounds. (**G**) Western blot analysis of LOX-IM-VI cells stably transfected with scrambled shRNA (sc, lane 1) or shRNA-hnRNP A18 (shA18, lane 2). Fold induction for TRX was calculated by densitometry and normalized to Actin (C–F) or GAPDH (G).

Moreover, the protein levels of hnRNP A18 expressed in PC3 tumor grown in mice correspond to CTLA-4 levels (Figure 6C). Most importantly, the chemical probes targeting hnRNP A18 decreased CTLA-4 expression in PC-3, LOX-IM-VI melanoma and MiaPaca pancreatic cancer cells in a dose-dependent manner (Figure 6D–G). These chemical probes thus do not disrupt hnRNP A18 protein levels (Figure 5A) but rather prevent its binding to targeted transcripts (Figure 3A–D) and reduce levels of their encoded proteins (Figures 5C–F, 6D–G).

We next evaluated the potential therapeutic index of these compounds by first confirming the effect of hnRNP A18 on cancer progression in a mouse model of human breast cancer. The data shown in Figure 7A and B indicate that down-regulation of hnRNP A18 significantly reduced MDA-MB-231 breast cancer progression and metastasis to the lungs. These data are in good agreement with our previous report on the effect of hnRNP A18 on melanoma and breast cancer progression *in vitro* and *in vivo* (5).

We then measured the effect of the compounds on the viability of three other cancer cell types and on normal epithelial cells. Data shown in Figure 7C–F indicate that although there is some drug sensitivity variability between cancer cells, overall, chemical probes Chembridge 7646184 and Chembridge 6823240 were the most effective, killing all cancer cell lines tested without affecting the viability of normal human epithelial cells even at doses as high as 150 μM (Figure 7F). OTAVA 2192853 also had no significant effect on normal cells viability (Figure 7F) while preferentially killing cancer cells although less efficiently than Chembridge 7646184 and Chembridge 6823240 in most cancer cell lines (Figure 7C–E). VITAS STK508411 was the least effective in RKO, D54 and MiaPaca cells with some degree (20–40%) of toxicity to normal cells. These data thus suggest that the chemical probes identified here could contribute to elucidate the underexplored biological function of RNA-Binding Proteins in cancer cells proliferation and serve as valuable scaffolds for development of improved small molecules with a desirable therapeutic index.

DISCUSSION

One of the main challenges in cancer therapy is the resistance that often ensues following an initial response to current treatments. The underlying causes of resistance vary but often result from cancer cells bypassing the targeted pathway by adopting alternative mechanisms to maintain their growth and progression. Combined chemotherapies and modalities are regularly designed to counter compensatory mechanisms and harness cancer progression from different angles, but these approaches also combine the toxicity of the different agents. Agents that could simultaneously target selected key pathways essential for cancer cell progression and survival would thus be expected to minimize toxicity and potential resistance. In that regard we have identified chemical probes targeting hnRNP A18, a

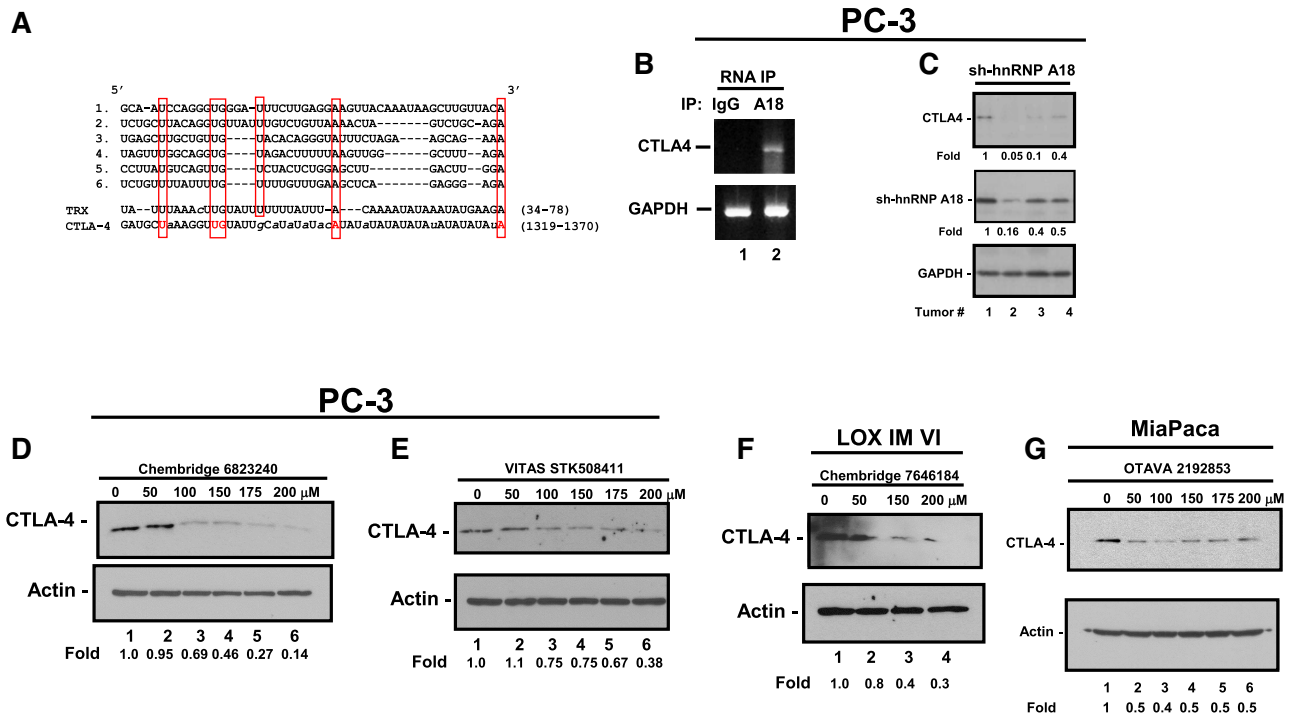

Figure 6. hnRNP A18 regulates CTLA-4 expression. (**A**) Sequence alignment of six possible versions (1-6) of the putative hnRNP A18 RNA recognition motif (11) and motif found in TRX and CTLA-4 3′UTR. Invariant nucleotides are in red boxes, and unmatched nucleotides are in *small caps italics*. The position of the hnRNP A18 recognition motif relative to the 3′-UTR start site is indicated in parentheses. (**B**) RNA-IP performed on prostate cancer PC-3 cells with the indicated antibody. CTLA-4 and GAPDH transcripts were reversed transcribed and amplified by PCR. (**C**) Western blots analysis of prostate cancer PC-3 cells grown in mice, individual tumor were excised and CTLA-4 and hnRNP A18 were detected. Fold induction was calculated by densitometry and normalized to GAPDH. (**D–G**) Western blot analysis of prostate cancer PC-3 (D, E), melanoma LOX-IM-VI (F) or pancreatic cancer MiaPaca (G) cells treated with increasing concentrations of the indicated compounds. Fold induction for CTLA-4 was calculated by densitometry and normalized to Actin.

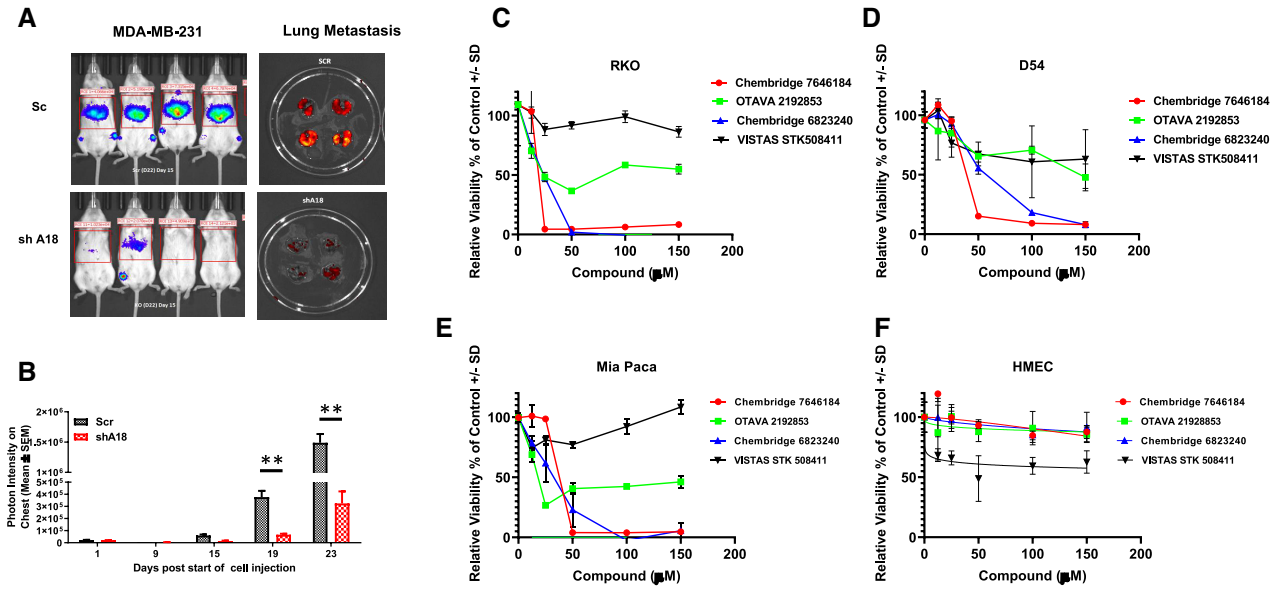

Figure 7. Potential therapeutic index of hnRNP A18 targeting. (**A**) Bioluminescence imaging (Xenogen IVIS) of human breast cancer MDA-MB-231 cells expressing the firefly luciferase gene and either scrambled shRNA (Sc) or shRNA hnRNP A18 (sh A18) and metastasis to the lungs. (**B**) Quantification of bioluminescence images in mice, $n = 4$. Bioluminescence was normalized to the initial signal (Day 1 of the respective group) and scrambled shRNA (Scr, black boxes) signals were compared to the shRNA hnRNP A18 (shA18, red boxes) signals at the indicated intervals. $^{**}P < 0.005$, Student's t-test. (**C–F**) Cell viability performed on colorectal carcinoma RKO (C), Glioblastoma D54 (D), pancreatic cancer MiaPaca (E) and normal human mammary epithelial HMEC (F) cells in the presence of increasing concentrations of Chembridge 7646184 (red line), Chembridge 6823240 (blue line), VITAS STK508411 (black line) and OTAVA 2192853 (green line). Error bars indicate standard deviation, $n = 3$.

regulator of protein translation in cancer cells. hnRNP A18 targets transcripts that are involved in cancer progression, metastasis, angiogenesis, anti-apoptosis and tumor immune checkpoint ((5), CTLA-4 Figure 6).

Although perturbations of RBP–RNA activity have been associated with cancer progression, development of small molecules that could disrupt these interactions has been rather challenging mainly due to the notorious disordered domains of RBPs and the flexibility of the RNA molecules (36). Nonetheless, these complexities endow RBPs the versatility required to control the metabolism of a large array of transcripts transcending more than one cancer hallmark (37). Because RBPs disordered domains are primarily associated with the RGG boxes, we focused our attention on the hnRNP A18 RRM to identify compounds that could disrupt hnRNP A18–RNA interactions. Using CADD based on SILCS, structural biology and cell-based assays we identified four chemical probes that specifically target hnRNP A18 RRM, disrupt its RNA binding activity, down regulate expression of targeted proteins, and selectively inhibit cancer cells proliferation (Figures 3–7). Our data indicate the hnRNP A18 regulates transcripts associated with cancer progression and an immune checkpoint through post-transcriptional regulation ((5,34) and Figure 6). Only a few drugs targeting protein synthesis are currently in development or in clinical use. All of them though target components of the general translational machinery that are also essential to normal cells and therefore conducive to toxicity and resistance. For example, homoharringtonine (HHT; Synribo, omacetaxine mepesuccinate) binds to the 80S ribosome in eukaryotic cells and inhibits protein synthesis by interfering with chain elongation (38). Rapamycin and its analogues, whose mechanism is PI3K/mTOR inhibition, inhibit the initiation of step cap-dependent translation (39). However, under stress and hypoxia, cap-independent initiation predominates making cells refractory to mTOR/PI3K inhibitors. In contrast, hnRNP A18 inhibitors are not expected to be affected by these conditions since hnRNP A18, which is over expressed under hypoxic conditions (5), functions through a different mechanism involving recognition of an RNA signature motif within the 3′UTRs of its targeted transcripts.

Combining protein translation inhibitors with immune checkpoint inhibitors is an attractive strategy that is currently being studied in pre-clinical and clinical settings (40) (NCT02423954, and NCT02890069, clinicaltrials.gov), but there is currently no single molecule that can accomplish these two biological functions. As mentioned above, the current approaches target the general protein translation machinery and are limited by drug dosing, optimal scheduling and added toxicity. For instance, humanized anti-CTLA-4 antibodies have shown impressive results in various tumors including melanoma and small cell lung cancer but can also induce significant immune-related adverse events (IRAE) such as colitis, dermatitis or endocrinopathies (41). Although CTLA-4 is primarily located in intracellular compartments, only a small proportion is rapidly recycled to the cell surface to mediate major inhibitory effects on T-cell activation (41). Interestingly, vaccines generated against hnRNP A18 (CIRP) resulted in stronger *in vivo* T-cell responses (42). Inhibiting CTLA-4 translation thus provides an alternative mechanism to increase cytotoxic T-cells activity against tumor antigen while preventing or reducing IRAE. The chemical probes identified here show specificity and efficacy against hnRNP A18 RNA binding activity *in vitro* and in cells. Based on hnRNP A18 low abundance in normal cells (5) we expected these probes to show preferential killing of cancer cells over normal cells. Indeed, our data support this expectation (Figure 7) and indicate that these chemical probes could serve as templates to better understand the underexplored biological function of RNA-RBPs interactions in cancer cells proliferation, elucidate new mechanisms to simultaneously inhibit cancer cells proliferation and an immune checkpoint and develop a new generation of anticancer agents with suitable therapeutic index.

DATA AVAILABILITY

The crystal structure of the hnRNP A18 RRM domain is publicly available through Protein Data Bank (PDB ID:5TBX). Backbone chemical shift assignments for the RRM domain of hnRNP A18 were obtained using standard heteronuclear multidimensional NMR experiments for double labelled ^{13}C-^{15}N-labeled hnRNP A18 RRM and deposited in the Biological Magnetic Resonance Database (BRMB; access number 28117).

SUPPLEMENTARY DATA

Supplementary Data are available at NAR Online.

ACKNOWLEDGEMENTS

The authors would like to thank Madeline Wilson for her technical assistance with fluorescence anisotropy experiments and the University of Maryland Marlene and Stewart Greenebaum Comprehensive Cancer Center Translational Laboratory Shared Services for animal work and cell viability assays. US Provisional Patent: 62/851 704 pending: 'First in class selective Small molecule inhibitors of hnRNP A18 to inhibit protein translation and immune checkpoint in cancer cells'.

FUNDING

National Institutes of Health [RO1CA177981-01 to F.C., D.J.W., R35GM131710 to A.D.M., in part]; University of Maryland Computer-Aided Drug Design Center, funds from the Center for Biomolecular Therapeutics (CBT) (to D.J.W.); Center for Maryland Advanced Ventures Life Sciences I.P. Fund (to F.C.); Maryland Department of Health's Cigarette Restitution Fund Program.
Conflict of interest statement. A.D.M. Jr, is co-founder and Chief Scientific Officer of SilcsBio LLC.

REFERENCES

1. Scheper,G.C., van der Knaap,M.S. and Proud,C.G. (2007) Translation matters: protein synthesis defects in inherited disease. *Nat. Rev. Genet.*, **8**, 711–723.
2. Cam,H. and Houghton,P.J. (2011) Regulation of mammalian target of rapamycin complex 1 (mTORC1) by hypoxia: causes and consequences. *Target Oncol.*, **6**, 95–102.

3. Pamboukian,R. and Carrier,F. (2012) hnRNP A18: a new pathway to regulate protein translation in cancer cells. *Mol. Cell. Pharm.*, **4**, 41–48.
4. Pereira,B., Billaud,M. and Almeida,R. (2017) RNA-binding proteins in cancer: old players and new actors. *Trends Cancer*, **3**, 506–528.
5. Chang,E.T., Parekh,P.R., Yang,Q., Nguyen,D.M. and Carrier,F. (2016) Heterogenous ribonucleoprotein A18 (hnRNP A18) promotes tumor growth by increasing protein translation of selected transcripts in cancer cells. *Oncotarget*, **7**, 10578–10593.
6. Fornace,A.J. Jr, Alamo,I. Jr and Hollander,M.C. (1988) DNA damage-inducible transcripts in mammalian cells. *Proc. Natl. Acad. Sci. U.S.A.*, **85**, 8800–8804.
7. Sheikh,M.S., Carrier,F., Papathanasiou,M.A., Hollander,M.C., Zhan,Q., Yu,K. and Fornace,A.J. Jr (1997) Identification of several human homologs of hamster DNA damage-inducible transcripts. Cloning and characterization of a novel UV-inducible cDNA that codes for a putative RNA-binding protein. *J. Biol. Chem.*, **272**, 26720–26726.
8. Nishiyama,H., Itoh,K., Kaneko,Y., Kishishita,M., Yoshida,O. and Fujita,J. (1997) A glycine-rich RNA-binding protein mediating cold-inducible suppression of mammalian cell growth. *J. Cell Biol.*, **137**, 899–908.
9. Yang,C. and Carrier,F. (2001) The UV-inducible RNA-binding protein A18 (A18 hnRNP) plays a protective role in the genotoxic stress response. *J. Biol. Chem.*, **276**, 47277–47284.
10. Wellmann,S., Buhrer,C., Moderegger,E., Zelmer,A., Kirschner,R., Koehne,P., Fujita,J. and Seeger,K. (2004) Oxygen-regulated expression of the RNA-binding proteins RBM3 and CIRP by a HIF-1-independent mechanism. *J. Cell Sci.*, **117**, 1785–1794.
11. Yang,R., Zhan,M., Nalabothula,N.R., Yang,Q., Indig,F.E. and Carrier,F. (2010) Functional significance for a heterogenous ribonucleoprotein A18 signature RNA motif in the 3′-untranslated region of ataxia telangiectasia mutated and Rad3-related (ATR) transcript. *J. Biol. Chem.*, **285**, 8887–8893.
12. Guvench,O. and MacKerell,A.D. Jr (2009) Computational fragment-based binding site identification by ligand competitive saturation. *PLoS Comput. Biol.*, **5**, e1000435.
13. Raman,E.P., Yu,W., Guvench,O. and Mackerell,A.D. (2011) Reproducing crystal binding modes of ligand functional groups using site-identification by ligand competitive saturation (SILCS) simulations. *J. Chem. Inf. Model.*, **51**, 877–896.
14. Raman,E.P., Yu,W., Lakkaraju,S.K. and MacKerell,A.D. Jr (2013) Inclusion of multiple fragment types in the site identification by ligand competitive saturation (SILCS) approach. *J. Chem. Inf. Model.*, **53**, 3384–3398.
15. Lakkaraju,S.K., Raman,E.P., Yu,W. and MacKerell,A.D. Jr (2014) Sampling of organic solutes in aqueous and heterogeneous environments using oscillating excess chemical potentials in grand canonical-like monte carlo-molecular dynamics simulations. *J. Chem. Theory Comput.*, **10**, 2281–2290.
16. Yu,W., Lakkaraju,S.K., Raman,E.P., Fang,L. and MacKerell,A.D. Jr (2015) Pharmacophore modeling using site-identification by ligand competitive saturation (SILCS) with multiple probe molecules. *J. Chem. Inf. Model.*, **55**, 407–420.
17. Coburn,K., Melville,Z., Aligholizadeh,E., Roth,B.M., Varney,K.M., Carrier,F., Pozharski,E. and Weber,D.J. (2017) Crystal structure of the human heterogeneous ribonucleoprotein A18 RNA-recognition motif. *Acta Crystallogr. F Struct. Biol. Commun.*, **73**, 209–214.
18. Word,J.M., Lovell,S.C., Richardson,J.S. and Richardson,D.C. (1999) Asparagine and glutamine: using hydrogen atom contacts in the choice of side-chain amide orientation. *J. Mol. Biol.*, **285**, 1735–1747.
19. Van Der Spoel,D., Lindahl,E., Hess,B., Groenhof,G., Mark,A.E. and Berendsen,H.J. (2005) GROMACS: fast, flexible, and free. *J. Comput. Chem.*, **26**, 1701–1718.
20. Best,R.B., Zhu,X., Shim,J., Lopes,P.E., Mittal,J., Feig,M. and Mackerell,A.D. Jr (2012) Optimization of the additive CHARMM all-atom protein force field targeting improved sampling of the backbone phi, psi and side-chain chi(1) and chi(2) dihedral angles. *J. Chem. Theory Comput.*, **8**, 3257–3273.
21. MacKerell,A.D., Bashford,D., Bellott,M., Dunbrack,R.L., Evanseck,J.D., Field,M.J., Fischer,S., Gao,J., Guo,H., Ha,S. *et al.* (1998) All-atom empirical potential for molecular modeling and dynamics studies of proteins. *J. Phys. Chem. B*, **102**, 3586–3616.
22. Vanommeslaeghe,K., Hatcher,E., Acharya,C., Kundu,S., Zhong,S., Shim,J., Darian,E., Guvench,O., Lopes,P., Vorobyov,I. *et al.* (2010) CHARMM general force field: A force field for drug-like molecules compatible with the CHARMM all-atom additive biological force fields. *J. Comput. Chem.*, **31**, 671–690.
23. Yu,W., He,X., Vanommeslaeghe,K. and MacKerell,A.D. Jr (2012) Extension of the CHARMM general force field to sulfonyl-containing compounds and its utility in biomolecular simulations. *J. Comput. Chem.*, **33**, 2451–2468.
24. Jorgensen,W.L., Chandrasekhar,J., Madura,J. D., Impey,R. W. and Klein,M. L. (1983) Comparison of simple potential functions for simulating liquid water. *J. Chem. Phys.*, **79**, 926–935.
25. Koes,D.R. and Camacho,C.J. (2011) Pharmer: efficient and exact pharmacophore search. *J. Chem. Inf. Model.*, **51**, 1307–1314.
26. Oashi,T., Ringer,A.L., Raman,E.P. and Mackerell,A.D. (2011) Automated selection of compounds with physicochemical properties to maximize bioavailability and druglikeness. *J. Chem. Inf. Model.*, **51**, 148–158.
27. Kansy,M., Senner,F. and Gubernator,K. (1998) Physicochemical high throughput screening: parallel artificial membrane permeation assay in the description of passive absorption processes. *J. Med. Chem.*, **41**, 1007–1010.
28. Sambrook,J.a.R. and D,W. (2006). In: Sambrook,J. and Russell,D.W. (eds). *The condensed protocols from Molecular cloning : a laboratory manual*, Cold Spring Harbor Laboratory Press, NY.
29. Delaglio,F., Grzesiek,S., Vuister,G.W., Zhu,G., Pfeifer,J. and Bax,A. (1995) NMRPipe: a multidimensional spectral processing system based on UNIX pipes. *J. Biomol. NMR*, **6**, 277–293.
30. Zucconi,B.E. and Wilson,G.M. (2013) Assembly of functional ribonucleoprotein complexes by AU-rich element RNA-binding protein 1 (AUF1) requires base-dependent and -independent RNA contacts. *J. Biol. Chem.*, **288**, 28034–28048.
31. Chou,M.Y., Rooke,N., Turck,C.W. and Black,D.L. (1999) hnRNP H is a component of a splicing enhancer complex that activates a c-src alternative exon in neuronal cells. *Mol. Cell. Biol.*, **19**, 69–77.
32. Burd,C.G. and Dreyfuss,G. (1994) RNA binding specificity of hnRNP A1: significance of hnRNP A1 high-affinity binding sites in pre-mRNA splicing. *EMBO J.*, **13**, 1197–1204.
33. Lopez de Silanes,I., Stagno d'Alcontres,M. and Blasco,M.A. (2010) TERRA transcripts are bound by a complex array of RNA-binding proteins. *Nat. Commun.*, **1**, 33.
34. Yang,R., Weber,D.J. and Carrier,F. (2006) Post-transcriptional regulation of thioredoxin by the stress inducible heterogenous ribonucleoprotein A18. *Nucleic Acids Res.*, **34**, 1224–1236.
35. Beusch,I., Barraud,P., Moursy,A., Clery,A. and Allain,F.H. (2017) Tandem hnRNP A1 RNA recognition motifs act in concert to repress the splicing of survival motor neuron exon 7. *Elife*, **6**, e25736.
36. Thomas,J.R. and Hergenrother,P.J. (2008) Targeting RNA with small molecules. *Chem. Rev.*, **108**, 1171–1224.
37. Hanahan,D. and Weinberg,R.A. (2011) Hallmarks of cancer: the next generation. *Cell*, **144**, 646–674.
38. Novotny,L., Al-Tannak,N.F. and Hunakova,L. (2016) Protein synthesis inhibitors of natural origin for CML therapy: semisynthetic homoharringtonine (Omacetaxine mepesuccinate). *Neoplasma*, **63**, 495–503.
39. Showkat,M., Beigh,M.A. and Andrabi,K.I. (2014) mTOR signaling in protein translation regulation: implications in cancer genesis and therapeutic interventions. *Mol. Biol. Int.*, **2014**, 686984.
40. Langdon,S., Hughes,A., Taylor,M.A., Kuczynski,E.A., Mele,D.A., Delpuech,O., Jarvis,L., Staniszewska,A., Cosulich,S., Carnevalli,L.S. *et al.* (2018) Combination of dual mTORC1/2 inhibition and immune-checkpoint blockade potentiates anti-tumour immunity. *Oncoimmunology*, **7**, e1458810.
41. Schneider,H. and Rudd,C.E. (2014) Diverse mechanisms regulate the surface expression of immunotherapeutic target ctla-4. *Front. Immunol.*, **5**, 619.
42. Villanueva,L., Silva,L., Llopiz,D., Ruiz,M., Iglesias,T., Lozano,T., Casares,N., Hervas-Stubbs,S., Rodriguez,M.J., Carrascosa,J.L. *et al.* (2018) The Toll like receptor 4 ligand cold-inducible RNA-binding protein as vaccination platform against cancer. *Oncoimmunology*, **7**, e1409321.